Geothermal Energy

RESEARCH Open Access

Study on the evolution of mechanical properties of hot dry rocks after supercritical CO_2 injection

Pan Li[1,2*], Hongxue Zhang[1*] and Yu Wu[2]

*Correspondence:
plee@cumt.edu.cn;
hxzhang@aust.edu.cn

[1] School of Mechanics and Optoelectronics Physics, Anhui University of Science and Technology, No. 168 Taifeng Road, Huainan 232001, Anhui, China
[2] State Key Laboratory for Geomechanics and Deep Underground Engineering, China University of Mining and Technology, Xuzhou 221116, Jiangsu, China

Abstract

Characterizing the evolution of mechanical properties of hot dry rock (HDR) after supercritical CO_2 (CO_2(sc)) injection is crucial for assessing the heat extraction rate and reservoir security of CO_2 based enhanced geothermal systems. This study designed the experiments of triaxial seepage and mechanical properties considering no CO_2(sc) injection, CO_2(sc) injection, and alternating injection of water-CO_2(sc) (AIWC) in granite at 150–300 ℃. The experiments can reveal the mechanical properties of HDR in single-phase CO_2 zone, CO_2-water two-phase zone and dissolved CO_2 liquid phase zone in HDR reservoir. The results indicate that the failure mode of the rock samples primarily exhibits sudden instability after no CO_2(sc) injection and AIWC, whereas it predominantly manifests progressive instability after CO_2(sc) injection. Compared with 25 ℃, the uniaxial compressive strength (UCS) after no CO_2(sc) injection at 150–300 ℃ decreased by 13.86%–32.92%. After CO_2(sc) injection, the UCS decreased by 40.79%–59.60%. After AIWC, the UCS decreased by 27.74–40.48%. This shows that the strength of rock mass in the single-phase CO_2 zone is lower than that in the other two zones, and this weakening phenomenon increases with the increase of temperature difference. At the same temperature, the elasticity modulus after AIWC was greater than that after no CO_2(sc) injection and CO_2(sc) injection. With no CO_2(sc) injection, when the temperature was increased to 200 ℃ and 300 ℃, intergranular cracks and transgranular appeared respectively. After AIWC, mineral crystals such as calcite were precipitated on the surfaces of the connected large cracks, accompanied by kaolinite clay minerals. This increases the frictional contact of the mineral particles and enhances the stability of the HDR reservoir.

Keywords: Granite, Supercritical CO_2, Thermal stress, Chemical effect, Microstructure

Introduction

Hot dry rock (HDR) geothermal energy is a low-carbon renewable energy with abundant reserves. The use of supercritical CO_2 (CO_2(sc)) instead of water as a heat extraction fluid can make HDR reservoirs potential geological carbon sinks (Brown 2000; Xu et al. 2014a). After a fractured reservoir is formed in the HDR via hydraulic fracturing, a small amount of CO_2 injected is dissolved in the fractured water during heat extraction. Under the water–CO_2–rock interaction, reservoir minerals dissolve and precipitate, such that

CO_2 is mineralized and stored as carbonate in the HDR reservoir (Fig. 1) (Wu et al. 2021). The CO_2(sc) injection and the resulting water–CO_2–rock interaction inevitably cause significant changes in multiple physical fields in the reservoir, including the stress, temperature, seepage, chemical, fracture, and energy fields (De Simone et al. 2013; Xie et al. 2015; Gao et al. 2024). These multifield coupling effects further affect the rock mass strength, elasticity modulus, porosity, permeability, and other mechanical properties of HDR (Li et al. 2023a; Yin et al. 2023). This may have two implications: (1) to enhance or deteriorate heat extraction and (2) to affect reservoir stability, such as by triggering earthquakes (Boyet et al. 2023; Cao et al. 2022; Jiang et al. 2022). Recently, many scholars have conducted fruitful studies on the mechanical properties of HDR under different conditions.

Granite is a dense hot rock mass widely distributed in deep strata and has great potential for geothermal exploitation (Li et al. 2023b). The injection of heat extraction fluid affects the mechanical properties of granite in two ways: (1) the generation and expansion of cracks caused by thermal stress and (2) the fluid–rock interaction caused by the chemical effect. The temperature change in granite caused by the injection of heat extraction fluid is a key factor causing thermal stress. The degradation of the mechanical properties of granite is largely attributed to the occurrence of intergranular and transgranular microcracks in the rock caused by thermal stress (Freire-Lista et al. 2016; Rong

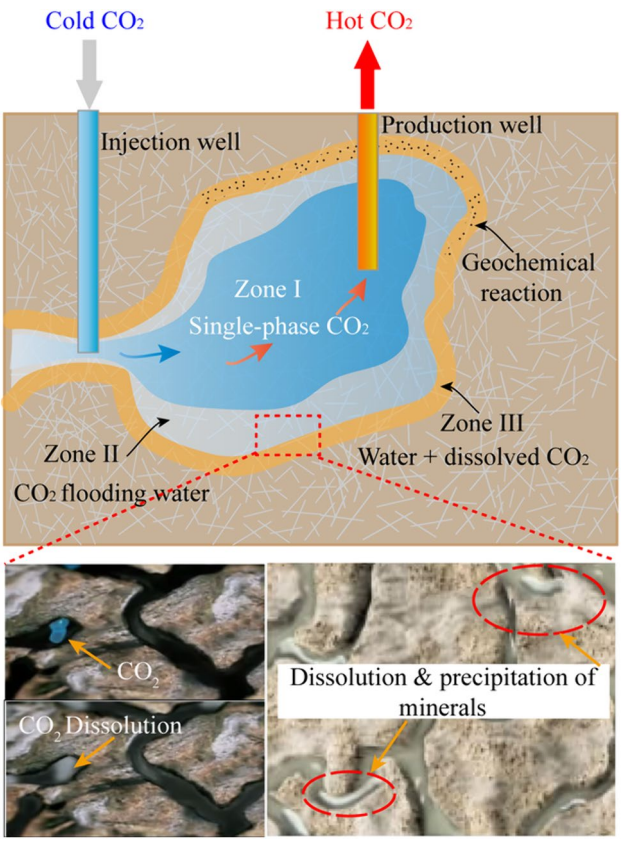

Fig. 1 Schematic diagram of CO_2 mineralization storage in a hot dry rock (HDR) reservoir (adapted from Ueda et al. (2005) and Wu et al. (2020))

et al. 2018). A previous study suggested that increasing the temperature releases both free and bound water in granite, which reduces the relative sliding between rock particles and increases the peak stress (Gautam et al. 2018). When the temperature rises from 25 ℃ to 400 ℃, the granite hardens owing to the loss of bound water, and its peak axial stress increases (Liu and Xu 2015; Wang et al. 2020). When the temperature exceeds 400 ℃, the mineral-bound water separates from the mineral skeleton, causing the decomposition and phase transition of the mineral. When the thermal stress exceeds the mineral bonding strength, it expands the thermal damage area, and reduces the strength of the rock mass (Wu et al. 2023; Zhang et al. 2016). Additionally, increasing the temperature can considerably reduce the roughness and improve the permeability of the fracture, which is conducive to heat transfer (Fang et al. 2018; Liu et al. 2023). Some studies have demonstrated that there are temperature thresholds for the changes in the mechanical properties and thermal damage of granite. In the non-stress state, the temperature threshold is 400 ℃, and when the confining pressure is increased to 75 MPa, the temperature threshold is reduced to 150 ℃ (Sun et al. 2015; Zhao et al. 2017). When the temperature is lower than 450 ℃, a small number of tensile cracks appear at the boundary of quartz and feldspar. When the temperature exceeds 450 ℃, many tensile cracks appear inside the mineral particles (Wang et al. 2023). Moreover, high temperatures affect the granite fracture form. When the temperature exceeds 600 ℃, the granite exhibits ductile failure, resulting in a brittle–plastic transition between 600 ℃ and 700 ℃ (Guo et al. 2023; Li et al. 2022). In addition to the temperature changes, the mineral microstructure of granite is also a factor that generates thermal stress. For granites containing a variety of minerals, increasing the temperature causes uncoordinated thermal expansion between the mineral crystals, resulting in thermal stress. However, the degree of impact of this process depends on the mineral content, mineral particle size, and shape (Shao et al. 2014; Vázquez et al. 2015; Yin et al. 2021).

Compared with the thermal stress, the chemical effect on the mechanical properties of granite is mainly reflected in the changes in the microstructure. When CO_2(sc) is injected into granite, it dissolves and ionizes in the geological water of the cracks, forming an acidic solution with a pH of approximately 4.3 (Truche et al. 2016). At this time, the crack surface is exposed to the acidic solution, and the water–CO_2–rock interaction occurs, resulting in the dissolution and precipitation of the minerals. This changes the microstructure of the granite, causing changes in its mechanical properties (Wu and Li 2020). Previous studies have shown that under CO_2(sc) saturation conditions, the mineral particle cementation and particle size in the granite are reduced, decreasing the uniaxial compressive strength (UCS) and elasticity modulus. The weakening of the strength and elasticity modulus of the granite is significantly dependent on the time of the water–CO_2–rock interaction (Isaka et al. 2019; Li et al. 2020). Simultaneously, chemical effects can significantly affect the permeability and porosity of granites: firstly, this effect depends on the type and content of the minerals. If the rock is rich in minerals such as calcite and silicates that are soluble in weak acids, the porosity response is dominated by mineral dissolution; otherwise, it is dominated by stress corrosion cracking (Kim and Makhnenko 2022); secondly, this effect is related to the fluid flow state. In the non-flowing state, the effect of CO_2 can generate clay minerals in the granite, causing blockage of cracks and reducing permeability (Ré et al. 2014). However, by stirring the CO_2–water

mixture to cause the solution to flow, it was found that the porosity and permeability of granite increased compared to those in the non-flowing state (An et al. 2023). Therefore, the temperature change and heat extraction fluid flow are important factors that affect the mechanical properties of HDR.

After CO_2 injection, the HDR reservoir is divided into single-phase CO_2 zone (zone I), CO_2-water two-phase zone (zone II) and dissolved CO_2 liquid phase zone (zone III) (Fig. 1). The zone II involves a CO_2 flooding water process and water–CO_2–rock interaction, but few experimental studies have reported the mechanical properties of HDR reservoirs considering the influence of CO_2 flooding water. This study designed the experiments of triaxial seepage and mechanical properties considering no CO_2(sc) injection, CO_2(sc) injection, and alternating injection of water-CO_2(sc) (AIWC) in granite at 150–300 ℃. The experiments can study the mechanical properties of rock mass in zone II and III.

In this study, by using high-temperature and high-pressure triaxial seepage experiment equipment and MTS816 rock mechanics test equipment from China University of Mining and Technology, the UCS, elasticity modulus, failure characteristics, and acoustic emission (AE) characteristics of granite under no CO_2(sc) injection, CO_2(sc) injection, and AIWC were studied at 150–300 ℃. The microstructure of the granite crack surface after AIWC was analyzed using a scanning electron microscope (SEM). The evolution of the mechanical properties of granite under the effects of temperature change and CO_2 flooding water flow was analyzed. The results provides technical guidance for assessing the heat extraction rate and reservoir security of HDR.

Methodology

Rock sample

The rock samples used in this study were obtained from high heat flow granite in Zhangzhou, Fujian Province, China. Fujian Province is the primary distribution area of high heat flow granites in China, with more than 70% of the land area consisting of high heat flow granites. The first HDR scientific drilling project in China was conducted in Zhangzhou (Zhuang 2016).

According to international rock mechanics test standards (Zheng et al. 2015), the obtained granite block was cut and polished to obtain a cylindrical standard specimen with a diameter of 50 mm and a height of 100 mm. The surface parallelism and flatness of the rock samples were within 0.05 mm and 0.02 mm, respectively. Subsequently, the wave velocities of the rock samples were measured using an ultrasonic instrument, and the rock samples with similar wave velocities were selected as the experimental samples for this study (Fig. 2). The measured wave velocities are shown in Table 1. Rock samples with wave velocity ranging from 3.833 to 4.348 km/s were selected in this study.

Experimental design and procedure

As shown in Fig. 3a, the experimental process consists of three parts. First, high-temperature and high-pressure triaxial seepage experiments were conducted on the rock samples. Then, the UCS and AE characteristics of the rock samples after seepage were tested. Finally, the microstructural changes on the crack surface were characterized in the AIWC experimental group. The specific experimental steps are as follows:

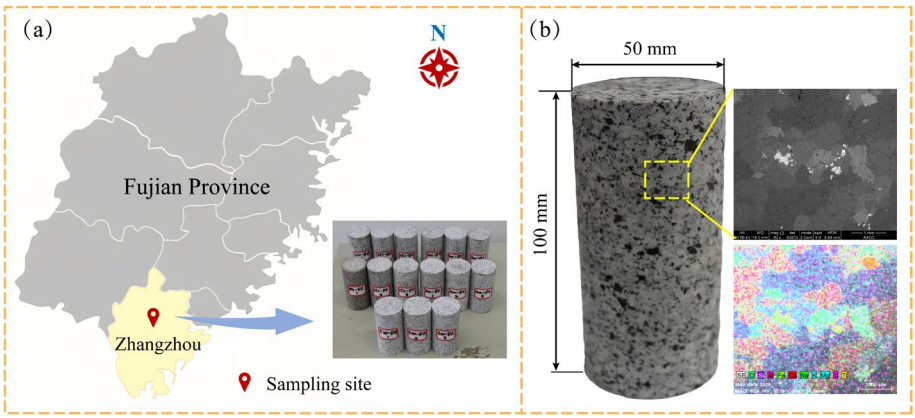

Fig. 2 **a** Sampling sites and **b** granite sample and its microscopic minerals

Table 1 Wave velocity of the rock sample

Rock sample No	Wave velocity (km/s)
1	3.571
2	4.000
3	4.255
4	4.348
5	3.226
6	3.849
7	4.194
8	4.219
9	3.760
10	3.537
11	4.258
12	4.318
13	3.833
14	4.034
15	4.307
16	4.223
17	4.290
18	3.869
19	3.478
20	4.288

(1) Experimental process for high-temperature and high-pressure triaxial seepage. First, cracks were created in the rock samples using the Brazilian splitting method, and then the rock samples were placed in a high-temperature and high-pressure triaxial seepage chamber (Fig. 3b). An axial pressure of 35 MPa and a confining pressure of 30 MPa were applied to the rock samples. Then four high-temperature scenarios (150 ℃, 200 ℃, 250 ℃, and 300 ℃) were set to represent the HDR reservoir temperature changes. Three fluid injection modes were established for each high-temperature scenario: no CO_2(sc) injection, CO_2(sc) injection, and AIWC.

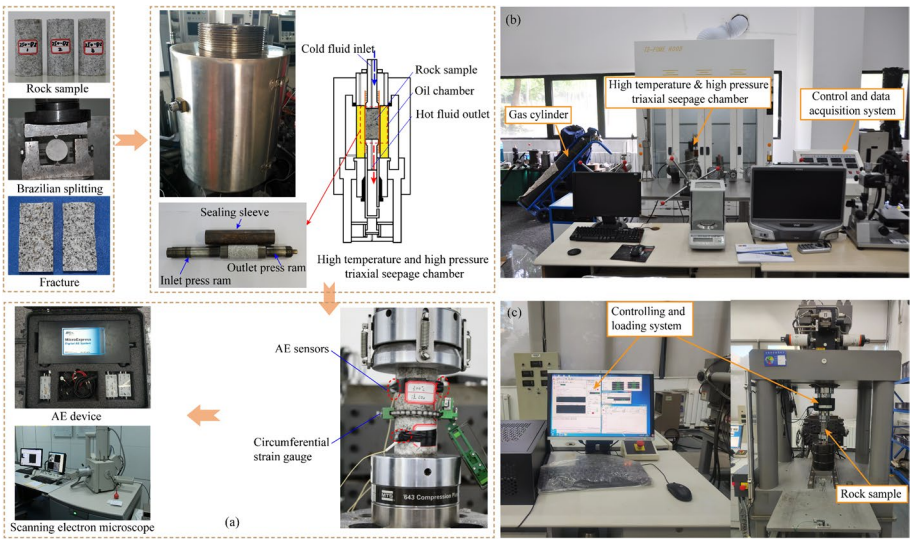

Fig. 3 **a** Experimental process design, **b** high temperature and high pressure triaxial seepage test equipment, and **c** MTS816 rock mechanics test equipment

During the experiment, CO_2 was injected at a temperature of 40 ℃ and a pressure of 7.5 MPa, while water was injected at an injection rate of 20 mL/min.

(2) UCS and AE tests. After the triaxial seepage test under each scenario, the rock samples were sealed with plastic wrap, and the UCS was tested using the mechanical experimental machine shown in Fig. 3c. A control group was set up at room temperature (25 ℃), and AE sensors were installed on the rock samples at 250 ℃ and 300 ℃ to monitor the AE characteristics during the UCS test. Thus, by collecting the load, deformation, and AE data during the experiment, the influence of different situations and different CO_2 injection forms on the rock sample strength and failure mechanism were analyzed.

(3) Observation and analysis of mineral microstructure on the crack surface. Bulk samples were collected at different positions of the cracks after AIWC, and changes in the mineral microstructure and composition on the crack surface were observed using SEM. Moreover, the type of reaction of the water–CO_2–rock interaction was revealed by analyzing the original mineral species in the vicinity where the mineral precipitation occurred. The SEM magnification can reach 1,000,000 times and the resolution can reach 3.0 nm.

High-temperature and high-pressure triaxial seepage test equipment

The high-temperature and high-pressure triaxial seepage test equipment used in this study was independently developed by the authors. The preparation of CO_2(sc) and the specific operation of the experiment were introduced by Wu et al. (2021). The experimental temperature and pressure of this equipment can reach 300 ℃ and 60 MPa, respectively. The experimental temperature of the rock sample was achieved by electric heating and an oil bath, and the rock sample was wrapped in a sleeve to isolate it from the high-temperature oil (Fig. 3a). The inlet and outlet press rams were

sealed with graphite rings. The experimental temperature and the pressure and temperature of the injected fluid were adjusted using a control system.

Results and analysis

Failure characteristics of uniaxial compression

Figure 4 illustrates the uniaxial compression test process and failure morphology of the rock sample after treatment at 25 ℃, 150 ℃, 200 ℃, 250 ℃, and 300 ℃, respectively. Based on the classification of granite failure morphology and modes at high temperatures by Xu et al. (2014b), it can be seen that the failure forms at 25 ℃ are mainly shear slips accompanied by cone cracks. After the three forms of CO_2(sc) injection at a temperature of 150 ℃, the rock sample failure modes included axial splitting, shear sliding, and axial splitting. Multi-layer cracking occurred along the axis when no CO_2(sc) injection was performed. At 200 ℃, the failure mode was mainly hourglass cone cracking after the three forms of CO_2(sc) injection. After CO_2(sc) injection or AIWC at 250 ℃, the failure mode was axial splitting, whereas cone cracking occurred after no CO_2(sc) injection. At 300 ℃, the failure mode was mainly axial splitting after no CO_2(sc) injection and CO_2(sc) injection, while it was shear slip after AIWC. After CO_2(sc) injection or AIWC, the failure mode of the rock sample varied. With no CO_2(sc) injection or AIWC, the failure mode was mainly sudden instability, whereas the failure mode after CO_2(sc) injection was mainly progressive instability.

Change of UCS

The stress–strain curves of the rock samples under uniaxial compression at different temperatures are presented in Fig. 5. After no CO_2(sc) injection at 25 ℃, 150 ℃, 200 ℃, 250 ℃, and 300 ℃, the peak strength of rock samples decreased from 182.78 MPa to 122.08 MPa with the increase in temperature, and the corresponding peak strain also gradually decreased.

Combining the failure modes of the rock samples and the stress–strain curves in Fig. 5, it can be found that the failure mode of the rock samples is mainly brittle fracture when the temperature does not exceed 300 ℃. Owing to the difference in the thermodynamic

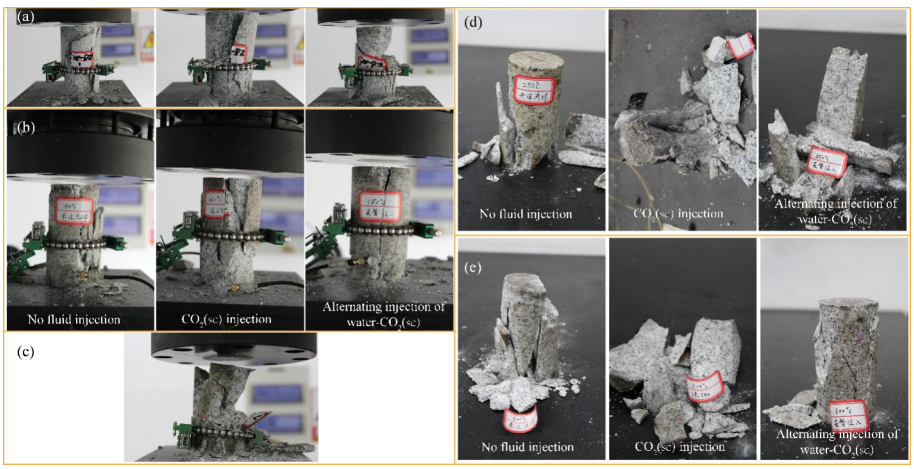

Fig. 4 Uniaxial compression test of rock samples at **a** 25 ℃, **b** 150 ℃, **c** 200 ℃, **d** 250 ℃, and **e** 300 ℃

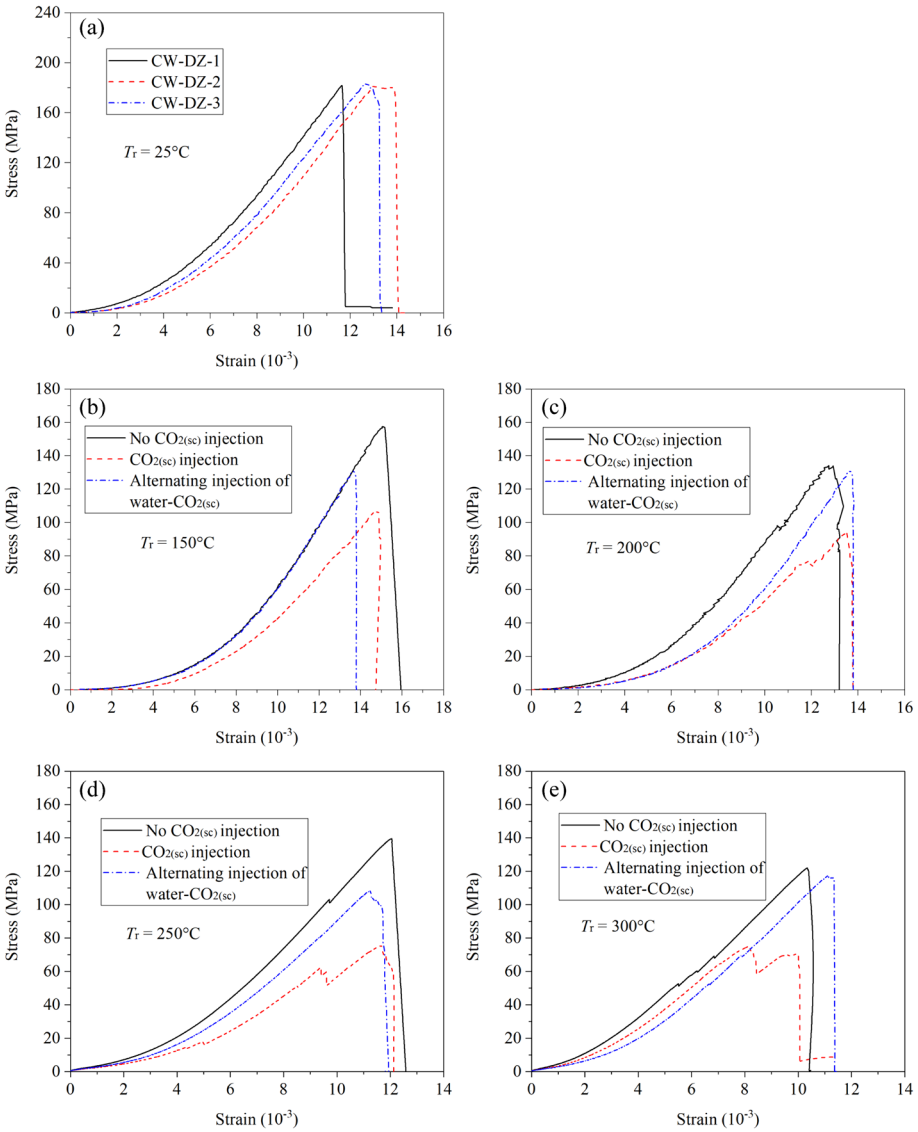

Fig. 5 Stress–strain curve of rock sample at **a** 25 ℃, **b** 150 ℃, **c** 200 ℃, **d** 250 ℃, and **e** 300 ℃

properties of different mineral crystals in the rock sample (such as the thermal expansion coefficient), the internal mineral particles undergo uncoordinated expansion at high temperatures, which easily produces small cracks and reduces their strength. Xu et al. (2014b) found that at high temperatures, three-dimensional tensile stress is generated inside the rock sample, resulting in intergranular cracks (below 200 ℃) or transgranular cracks (above 200 ℃). From the perspective of mineral crystal properties, the plasticity of mineral crystals increases with increasing temperature, which activates the properties of intercrystalline cement and decreases the overall strength of the rock samples (Xu et al. 2013).

However, the UCS of the rock samples after CO_2(sc) injection or AIWC was different from that after no CO_2(sc) injection. As shown in Fig. 5b to e, at the same temperature, the peak strength decreased successively after no CO_2(sc) injection, AIWC, and CO_2(sc)

injection. In addition, the change in peak strength with temperature after CO_2(sc) injection and AIWC was consistent with that after no CO_2(sc) injection; that is, the peak strength decreased with increasing temperature. Compared with 25 ℃, the UCS after no CO_2(sc) injection at 150–300 ℃ decreased by 13.86–32.92%. After CO_2(sc) injection, the UCS decreased by 40.79–59.60%. After AIWC, the UCS decreased by 27.74–40.48%. The reason for the above change in the peak strength is that the crack in the rock sample is stimulated by cold after the CO_2(sc) injection. The uncoordinated shrinkage of different mineral crystals results in crack damage, which reduces their strength. After AIWC, the cold stimulation process is accompanied by a water–rock–CO_2 interaction. In other words, the precipitation of minerals on the crack surface increases the frictional contact of the mineral particles, making their strength higher than that after CO_2(sc) injection.

Change in elasticity modulus

From the slope of the elastic stage of the stress–strain curve shown in Fig. 5b to e, the average elasticity modulus of the rock sample at 25 ℃ and 150–300 ℃ after the three forms of CO_2(sc) injection were obtained. The uniaxial compressive elasticity modulus of granite after no CO_2(sc) injection was compared with those in previous studies (Chen et al. 2012; Liu and Xu 2015; Miao et al. 2021), as shown in Fig. 6. Previous results suggest that the elasticity modulus of different granite samples decreases with an increase in temperature. In this study, the elasticity modulus decreased rapidly when the temperature increased to 150 ℃, which is due to the thermal expansion of mineral particles. The thermal stress generated by the uncoordinated thermal expansion of different minerals causes many microcracks, reducing the linear elastic behavior of granites (Liu and Xu 2015). It is worth noting that the elasticity modulus of the rock sample increased when the temperature increased from 200 ℃ to 250 ℃. This is because of the large loss of free and bound water in this temperature range, which reduces the relative sliding between the mineral grains, increasing the elasticity modulus. This result is consistent with that of Miao et al. (2021). It has been found

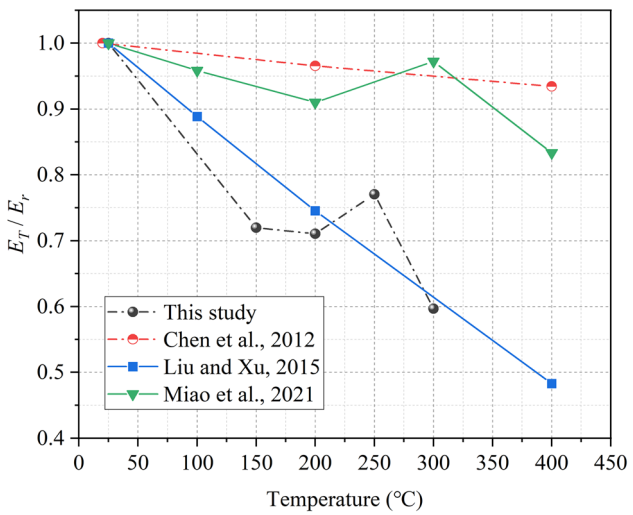

Fig. 6 Evolution of elasticity modulus with temperature after no CO_2(sc) injection (E_r is the elasticity modulus at 25 ℃, E_T is the elasticity modulus at various temperatures, and E_T/E_r is the normalized elasticity modulus)

that when the temperature exceeds 250 ℃, the cohesion of mineral grains decreases rapidly because of thermal softening, resulting in sliding and a sharp decline in the elasticity modulus (Gautam et al. 2018).

As expected, the injection of the heat extraction fluid significantly affected the elasticity modulus of the rock sample. Figure 7 shows the evolution of the elasticity modulus at different temperatures and fluid injection forms. At temperatures less than 200 ℃, the cooling shrinkage effect of CO_2(sc) injection is slightly greater than the thermal expansion effect, which reduces the effective contact between mineral particles and leads to a sharp reduction of the elasticity modulus. When the temperature exceeds 200 ℃, the thermal expansion effect of mineral particles is enhanced, which offsets most of the cooling shrinkage effect. Therefore, the decreasing trend of elasticity modulus slows down. After AIWC, at the same temperature, the elasticity modulus of the rock sample was higher than that after no CO_2(sc) injection and CO_2(sc) injection. However, the elasticity modulus exhibited a decreasing trend with increasing temperature. This is because the mineral dissolution causes mechanical damage to the rock skeleton, weakens the mechanical properties of the rock sample, and reduces its elasticity modulus. However, at the same time, the precipitation of insoluble minerals increases the contact between the mineral particles and makes the reduction of elasticity modulus not too large. When the temperature does not exceed 150 ℃, considering the flow effect of water and CO_2, there is less mineral precipitation in the connected large cracks, which is prone to relative sliding, leading to a decrease in the elasticity modulus (Wu and Li 2020). When the temperature rises to 150–200 ℃, the dissolution and precipitation of minerals are enhanced, and the mineral precipitation in large cracks is increased. This increases the contact between the mineral particles, resulting in a small increase in the elasticity modulus of the rock sample. When the temperature exceeds 200 ℃, the influence of temperature on the elasticity modulus is greater than the chemical effect. With an increase in temperature, the mineral grains slide relative to each other owing to thermal softening, resulting in a sharp decrease in the elasticity modulus.

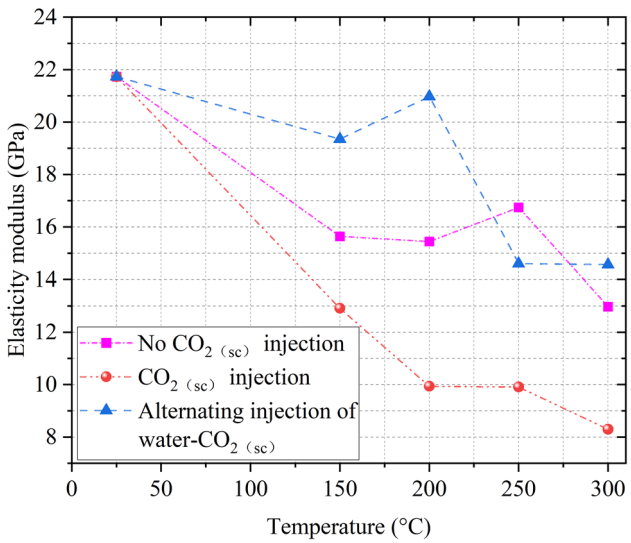

Fig. 7 Evolution of elasticity modulus at different temperatures and CO_2(sc) injection forms

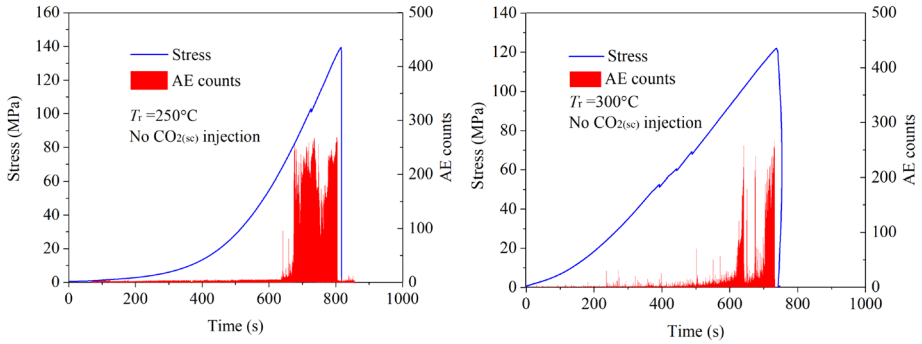

Fig. 8 Acoustic emission (AE) event counts at 250 ℃ (left) and 300 ℃ (right) after no CO_2(sc) injection

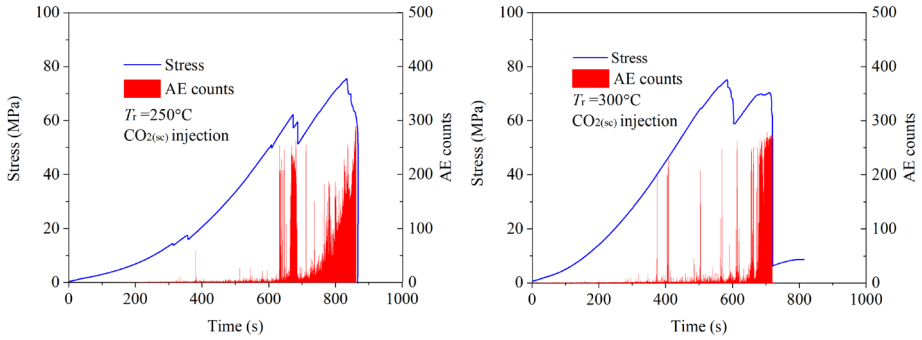

Fig. 9 Acoustic emission (AE) event counts at 250 ℃ (left) and at 300 ℃ (right) after CO_2(sc) injection

Change in AE

The AE event count and stress–strain curve correspondence can indirectly reflect the internal failure and energy release process of a rock sample (Tang et al. 2019), and the AE events are affected by the mineral particle size, major cracks, and lattice structure of rock samples (Kao et al. 2011). Figure 8 shows the AE event count during the uniaxial compression of rock samples at 250 ℃ and 300 ℃ after no CO_2(sc) injection (the horizontal coordinate in the figure replaces the strain with the corresponding time).

It can be seen that after no CO_2(sc) injection at 250 ℃ and 300 ℃, the cracks and micropores in the rock samples were gradually closed due to compression stress, and the micro-convex part of the cracks was squeezed and slipped, resulting in a small number of AE signals. In the linear elasticity stage, with an increase in temperature, the expansion of mineral particles at 300 ℃ was more significant than that at 250 ℃, and the change in the mineral lattice structure was significant, which reduced the energy release. As a result, there were more AE events at 250 ℃ than at 300 ℃ at this stage. When the stress reached its peak strength, a sudden brittle failure occurred in the rock sample, and the AE event count reached its maximum at both temperatures. Furthermore, a cone–crack failure mode occurred at 250 ℃, while at 300 ℃, the rock samples exhibited axial splitting failure mode.

Figure 9 shows the AE event count during uniaxial compression after CO_2(sc) injection at 250 ℃ and 300 ℃. After CO_2(sc) injection, the AE activity was not significant in the compaction stage of the rock sample. However, in the elastic stage, there were a

few relatively obvious AE signals at 250 ℃ and 300 ℃. Moreover, compared with the no CO_2(sc) injection condition, the strain proportion of the stress–strain curve at the yield stage increased at 250 ℃, and more significant AE signals were generated after local failure. With the continuous initiation and expansion of cracks, the AE signals continued to increase and appeared in large numbers near the peak strength. The stress–strain curve shows that at 300 ℃, a few obvious AE signals appeared at the peak strength, but the rock sample did not completely lose its bearing capacity. As the loading continued, cracks in the rock sample continued to expand, secondary cracks occurred, and several AE signals were generated. This further shows that after CO_2(sc) injection, cold stimulation affects the mineral crystal morphology of the rock samples and produces more microcracks; the higher the temperature of the rock samples, the greater the impact.

Figure 10 shows the AE event counts during uniaxial compression of the rock samples after AIWC at 250 ℃ and 300 ℃. Compared with CO_2(sc) injection and no CO_2(sc) injection, after AIWC, the AE events during the compaction stage increased at 250 ℃ and 300 ℃. This is because the cold stimulation of the AIWC causes changes in the mineral crystal volume of the rock samples. Simultaneously, the water–CO_2–rock interaction causes mineral dissolution and precipitation on the surfaces of cracks and micropores, resulting in changes in the mineral morphology and particle size on the surfaces of cracks and micropores. Therefore, under the combined effect of compressive stress and shear stress, dense convex structure extrusion and small dislocations occur on the surfaces of cracks and micropores, resulting in an increase in AE events; the higher the temperature, the more evident the increase. Compared with CO_2(sc) injection, the failure mode of the rock samples changed to sudden instability after AIWC, and the peak strength increased.

Microstructure change

The microstructure of pores and cracks significantly affects the mechanical properties of rocks. Increasing the temperature causes the development and expansion of pores and cracks and weakens the mechanical properties of the rock mass. Figure 11 illustrates the SEM images of the rock sample at temperatures of 150–300 ℃. At temperatures between 150 ℃ and 200 ℃, the free water inside the rock sample is lost with the increase in temperature, forming voids, but the thermal cracks are less (Fig. 11a). At 200 ℃ (Fig. 11b), the plastic properties of the mineral crystals increase, the properties of the

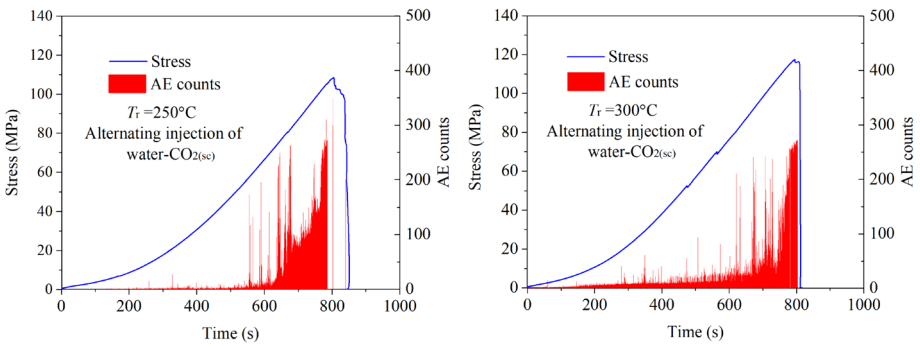

Fig. 10 Acoustic emission (AE) event counts at 250 ℃ (left) and at 300 ℃ (right) after alternating injection of water-CO_2(sc) (AIWC)

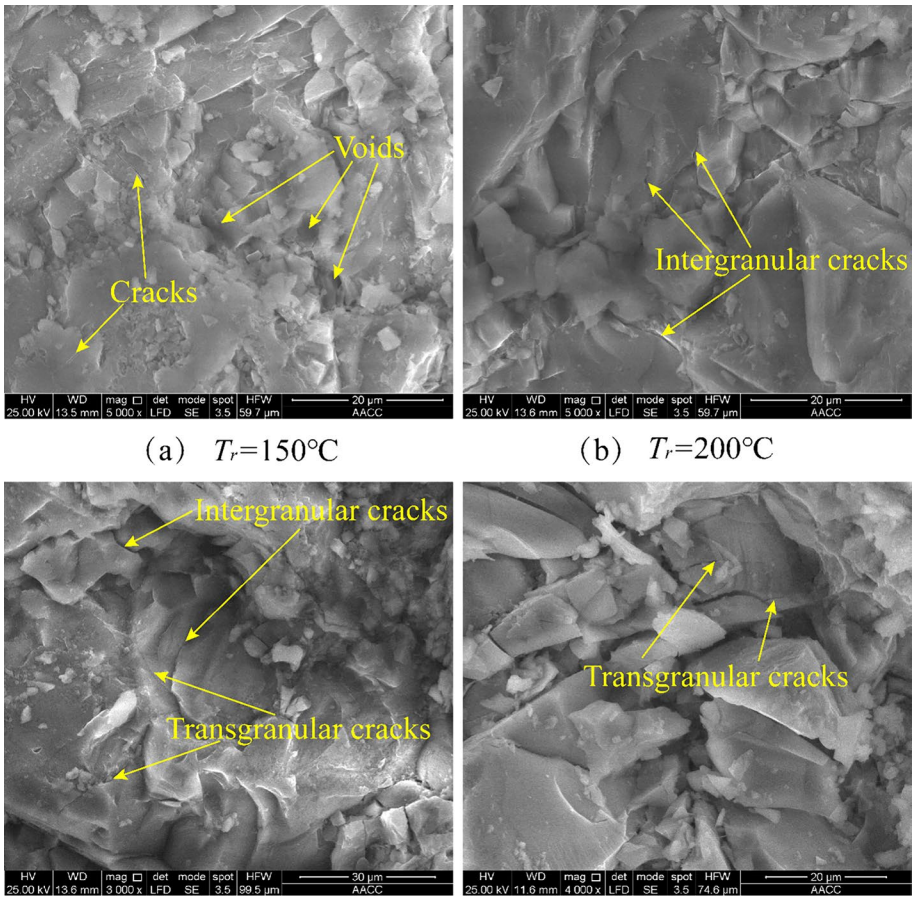

Fig. 11 SEM images of rock samples at temperatures of **a** 150 °C, **b** 200 °C, **c** 250 °C, and **d** 300 °C

intercrystalline cement are activated, and intergranular cracks occur along the crystal boundary. When the temperature exceeds 200 ℃, with the increase in temperature, the strongly bound water in minerals is lost and causes the decomposition and phase transition of mineral crystals (Zhang et al. 2016). Simultaneously, different mineral particles produce uncoordinated thermal expansion and generate many transgranular cracks (Figs. 11c and d). Transgranular cracks are connected with intergranular cracks to form a crack network, which significantly changes the integrity of the rock sample and affects its mechanical properties.

In addition, the crack microstructure is affected by the chemical effects after the injection of the heat extraction fluid at high temperatures. Figure 12 shows the SEM observation results of the crack surface after AIWC at 200 ℃. Because of water–CO_2–rock interaction, the skeletons of some easily soluble minerals (such as feldspar silicate minerals) dissolve, and the dissolved mineral particles gather near disconnected pores and cracks under the influence of flowing water–CO_2. These mineral particles further dissolve and precipitate new mineral crystals (such as calcite). This process may also be accompanied by the precipitation of clay minerals (such as kaolinite)

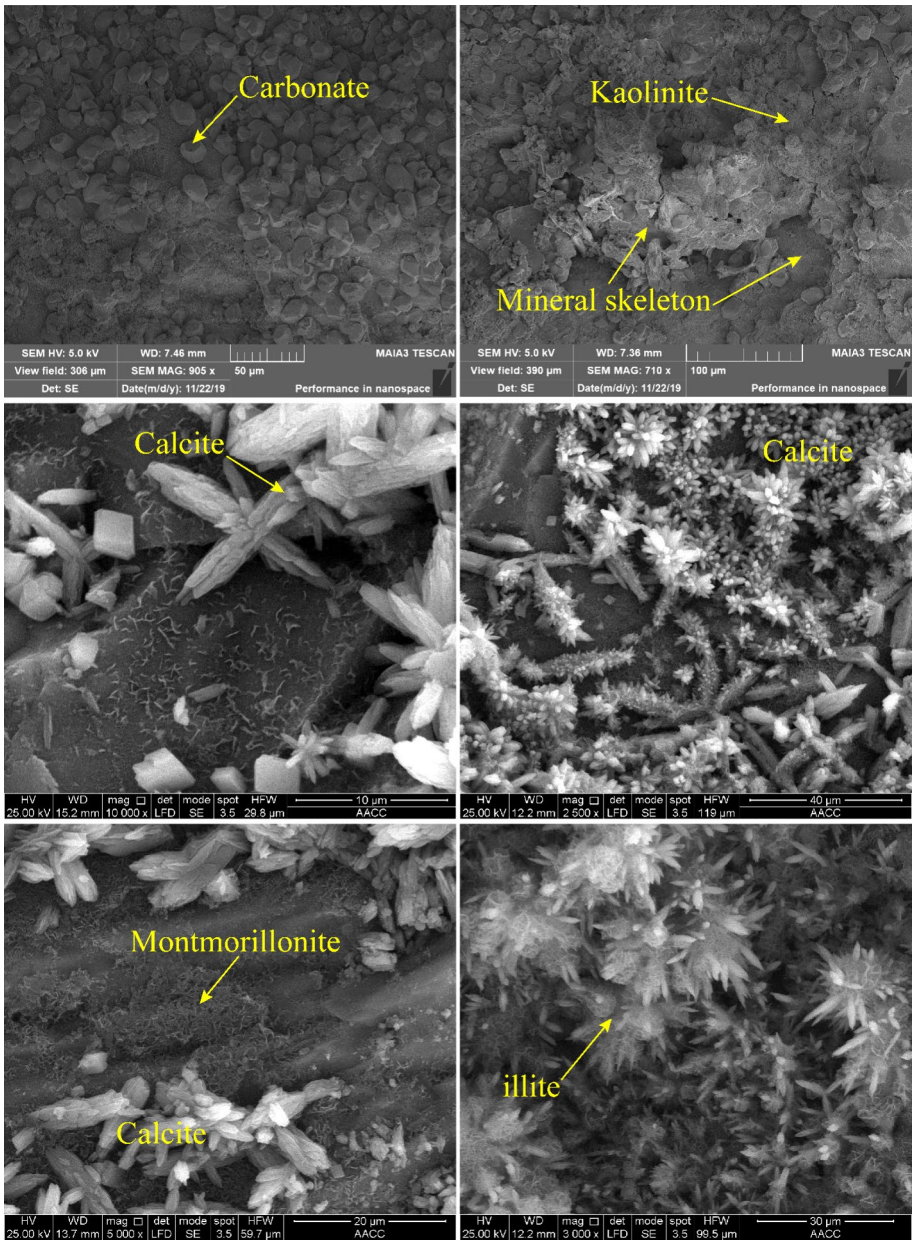

Fig. 12 SEM images of rock sample after alternating injection of water-CO_2(sc) (AIWC) at 200 ℃

(Wu et al. 2021). Due to the flow effect, the reaction range of the dissolved mineral skeleton is gradually deepened, intensifying the damage range. Therefore, the content and distribution of soluble and insoluble minerals in the crack surface dominate the mechanical damage of the rock sample (An et al. 2022). However, the solubility is relative, and the dissolution of minerals, such as quartz and biotite, is affected by temperature and ion concentration. As analyzed in Sect. "Change in elasticity modulus", when the temperature rises to 200 ℃, precipitation of minerals increases on the connected large crack surface, which increases the contact of mineral particles on the crack surface and enhances the strength of the rock sample.

Discussion

After AIWC at high temperatures, many carbonate mineral crystals are observed on the fracture surface, which increases the frictional contact between the mineral particles and enhances the strength of the rock samples. The CO_2 mineralization storage during this process is conducive to the stability of the HDR reservoir, as suggested by Yarushina and Bercovici (2013). They suggested that carbon storage in a rock mass is beneficial for reducing earthquake risk. Because mineral precipitation increases the contact area between solid particles, the effective fluid pressure is reduced, deviational stress is dispersed, and frictional contact is increased. Therefore, mineralization storage has the potential to reduce earthquake risk when fluid pumping rates do not exceed critical values.

Under the three CO_2(sc) injection conditions, the mechanical properties of the rock samples deteriorate with increasing temperature. After no CO_2(sc) injection, the rock sample experiences thermal stress caused by mineral thermal expansion. Granite is an aggregate composed of quartz, feldspar, mica, and other minerals, and the coefficient of thermal expansion of each mineral varies (Yin et al. 2021). Thus, when the temperature increases, mineral particles undergo uncoordinated thermal expansion, resulting in thermal stress in the rock sample (Wu et al. 2023). And the above phenomenon is also affected by mineral grain size. Figure 13 shows the influence of fine and coarse-grain size on the mechanical properties of granite (Shao et al. 2014). It is found that the peak load of coarse-grained granite is lower than that of fine-grained granite. And the difference gradually increases when the temperature exceeds 600 ℃. For the elasticity modulus, the granite mineral grain size has little influence on it within 400 ℃. When the temperature exceeds 400 ℃, the elasticity modulus of coarse-grained is smaller than that of fine-grained granite, and the difference increases gradually with the increase of temperature.

Simultaneously, an increase in temperature causes the loss of free and bound water in the rock sample, which activates the cement properties. When the thermal stress exceeds the limit, an intergranular crack appears at the crystal boundary of the mineral. As the temperature continues to increase, the strongly bound water in the mineral is lost, which causes the decomposition and phase transition of the mineral crystals, generating transgranular cracks (Zhang et al. 2016). However, at the same temperature, the UCS of the rock samples decreases after CO_2(sc) injection and AIWC compared to that

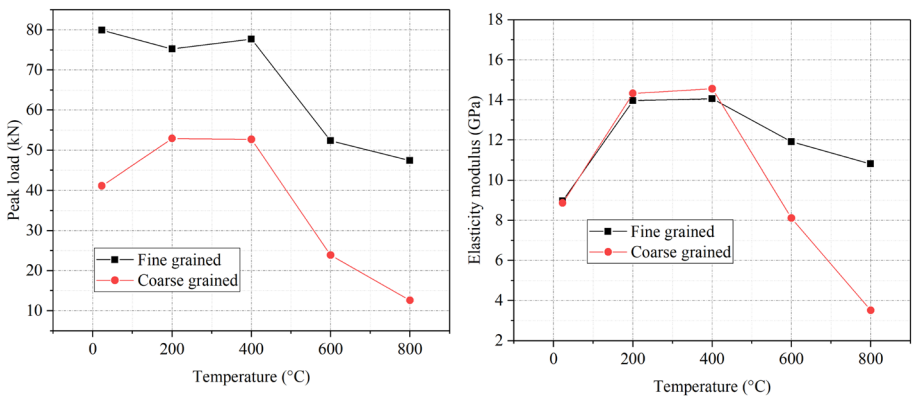

Fig. 13 Effect of granite grain size on peak load and elasticity modulus (adapted from Shao et al. (2014))

after no CO_2(sc) injection. This is because, in both cases, the thermal stress is controlled by the thermal expansion and cooling shrinkage of the mineral particles. Heat exchange occurs between the flowing CO_2 and the crack surface, such that the temperature of the crack surface drops quickly, while the temperature inside decreases more slowly. This temperature difference results in thermal stress. Consequently, tensile stress is generated outside the rock sample, and compressive stress is generated inside. Because the tensile strength of granite is less than its compressive strength, when the external tensile stress exceeds the internal compressive stress, the damaged crack further expands inward, aggravating the internal damage of the rock sample (Wu et al. 2023). However, the UCS of the rock samples after AIWC is greater than that after CO_2(sc) injection. Therefore, the stabilities of zones II and III of the HDR reservoir are slightly higher than that of zone I (see Fig. 1). The mineral crystallization in zones II and III reduces permeability and weakens heat extraction. Therefore, if the CO_2 injection pressure, flow rate, and temperature can be reasonably controlled to reduce reservoir damage in zone I and ensure the permeability of zones II and III, it is expected to improve the heat extraction rate and ensure the security of the reservoir.

The results of this study provide technical guidance for the safe and efficient exploitation of HDR. However, in this study, the rock samples were first treated with high temperature and CO_2 injection, and then their mechanical properties were tested. This cannot accurately reflect the real-time common effects of CO_2 flow and rock temperature/pressure in an actual HDR reservoir. Therefore, in future studies, it is necessary to consider the evolution of the mechanical properties of the rock sample in real-time triaxial high-temperature seepage processes to obtain more accurate results.

Conclusions

The injection of the heat extraction fluid affects the mechanical properties of the HDR reservoir and changes its permeability and stability. Studying the evolution of the mechanical properties of reservoir rock masses is important to ensure the efficient and safe exploitation of HDR geothermal energy. In this study, the UCS, AE characteristics, elasticity modulus, and microstructure changes of granite samples were tested under the three forms of CO_2(sc) injection at temperatures of 150–300 ℃. The failure mechanisms of the rock samples were analyzed under these different conditions. The main conclusions are as follows.

(1) At 25 ℃, the failure of the rock samples was primarily a shear slip accompanied by a cone crack. At temperatures of 150–300 ℃, after CO_2(sc) injection and AIWC, the failure mode of granite became variable. With no CO_2(sc) injection and AIWC, the failure mode of the rock sample was mainly sudden instability, whereas the failure mode after CO_2(sc) injection was mainly progressive instability.

(2) After the three forms of CO_2(sc) injection, the UCS of the rock samples decreased with an increase in temperature. Compared with 25 ℃, the UCS after no CO_2(sc) injection at 150 ℃, 200 ℃, 250 ℃, and 300 ℃ decreased by 13.86%, 26.15%, 23.29%, and 32.92%, respectively. After CO_2(sc) injection, the UCS decreased by 40.79%, 47.85%, 58.33%, and 59.60%, respectively. After AIWC, the UCS decreased by 27.74%, 27.86%, 40.48%, and 35.40%, respectively. Additionally, at the same temper-

ature, the peak strength of the rock sample decreased successively after no CO_2(sc) injection, AIWC, and CO_2(sc) injection.

(3) The elasticity modulus of the rock samples under the three CO_2(sc) injection scenarios generally showed a downward trend with an increase in temperature. However, the elasticity modulus increased slightly when the temperature increased from 200 ℃ to 250 ℃ after no CO_2(sc) injection. The same result occurred when the temperature increased from 150 ℃ to 200 ℃ after AIWC. In addition, at the same temperature, the elasticity modulus decreased successively after AIWC, no CO_2(sc) injection, and CO_2(sc) injection.

(4) After no CO_2(sc) injection, the AE events at 250 ℃ were more than that at 300 ℃, and the rock sample experienced a sudden brittle failure. Compared with the no CO_2(sc) injection, the proportion of strain at the yield stage of the stress–strain curve at 250 ℃ increased after CO_2(sc) injection, and more obvious AE signals were generated after local failure. At 300 ℃, the stress–strain curve of the rock sample showed a few obvious AE signals at the peak strength, but the rock sample did not completely lose its bearing capacity. At 250 ℃ and 300 ℃, the AE events during the compaction stage were increased after AIWC, compared with no CO_2(sc) injection and CO_2(sc) injection. Compared with CO_2(sc) injection, the failure mode of the rock samples changed to sudden instability after AIWC.

(5) After no CO_2(sc) injection, at 150–200 ℃, a few voids and thermal cracks occurred inside the rock sample. When the temperature was increased to 200 ℃, intergranular cracks occurred along the mineral crystal boundaries. When the temperature exceeded 200 ℃, many transgranular cracks appeared on the crack surface under the combined effect of mineral crystal decomposition/phase transformation and uncoordinated thermal expansion. Carbonate mineral crystals precipitated on the surfaces of the large connected cracks accompanied by clay minerals. This increased the contact between the mineral particles and enhanced the strength of the rock samples.

Abbreviations

HDR	Hot dry rock
CO_2(sc)	Supercritical CO_2
AIWC	Alternating injection of water-supercritical CO_2
UCS	Uniaxial compressive strength
AE	Acoustic emission
SEM	Scanning electron microscope

Acknowledgements

This work was supported by Scientific Research Foundation for High-level Talents of Anhui University of Science and Technology [grant number 13200394]; State Key Laboratory for Geomechanics and Deep Underground Engineering, China University of Mining and Technology [grant number SKLGDUEK2112]; the National Natural Science Foundation of China [grant number 52227901]; Anhui University Natural Science Foundation [grant number KJ2020A0329]; College students' innovation and entrepreneurship training program of Anhui Province [Grant Number S202310361186]. The authors furthermore thank the anonymous reviewers, Prof. Shao and other related editors who have significantly enhanced the quality of this paper.

Author contributions

PL measured and analyzed the data, prepared the figures, and wrote the first draft of the manuscript. HZ conducted some of the petrophysical measurements and microstructural investigations. YW helped in designing the study, contributed to the writing and the discussion of the results. All the authors read and approved the final manuscript.

Funding

Scientific Research Foundation for High-level Talents of Anhui University of Science and Technology, 13200394, Pan Li, State Key Laboratory for Geomechanics and Deep Underground Engineering,China University of Mining and Technology, SKLGDUEK2112, Pan Li, National Natural Science Foundation of China, 52227901, Anhui University Natural Science

Foundation, KJ2020A0329, Pan Li, College students' innovation and entrepreneurship training program of Anhui Province, S202310361186

Data availability
All data generated or analysed during this study are included in this published article.

Declarations

Competing interest
The authors have no conflicts of interest to declare.

Received: 6 April 2024 Accepted: 15 July 2024
Published online: 06 August 2024

References

An Q, Zhang Q, Zhang X, Li X, Yu H, Liu Y. Influence of mineralogy on rock mechanical behaviour considering dynamic alteration damage caused by SC-CO_2: a comparative study on different rock types. Rock Mech Rock Eng. 2022;55:3129–51. https://doi.org/10.1007/s00603-022-02807-w.

An Q, Zhang L, Zhang X, Zhang Q. Experiment on no-flow and flow CO_2-water–rock interaction: a kinetics calculation method for rock pore evolution. Chem Eng J. 2023;464:142754. https://doi.org/10.1016/j.cej.2023.142754.

Boyet A, De Simone S, Vilarrasa V. Physics-based modeling to understand and to propose forecasting methods of induced seismicity. Seismol Res Lett. 2023;94:2666–78. https://doi.org/10.1785/0220230109.

Brown DW. A hot dry rock geothermal energy concept utilizing supercritical CO_2 instead of water. In: Proceedings of the twenty-fifth workshop on geothermal reservoir engineering. Stanford University: Stanford. 2000. pp. 233–8.

Cao W, Durucan S, Shi JQ, Cai W, Korre A, Ratouis T. Induced seismicity associated with geothermal fluids re-injection: poroelastic stressing, thermoelastic stressing, or transient cooling-induced permeability enhancement? Geothermics. 2022;102:102404. https://doi.org/10.1016/j.geothermics.2022.102404.

Chen YL, Ni J, Shao W, Azzam R. Experimental study on the influence of temperature on the mechanical properties of granite under uni-axial compression and fatigue loading. Int J Rock Mech Min. 2012;56:62–6. https://doi.org/10.1016/j.ijrmms.2012.07.026.

De Simone S, Vilarrasa V, Carrera J, Alcolea A, Meier P. Thermal coupling may control mechanical stability of geothermal reservoirs during cold water injection. Phys Chem Earth. 2013;64:117–26. https://doi.org/10.1016/j.pce.2013.01.001.

Fang Y, Elsworth D, Ishibashi T, Zhang F. Permeability evolution and frictional stability of fabricated fractures with specified roughness. J Geophys Res-Sol Ea. 2018;123:9355–75. https://doi.org/10.1029/2018JB016215.

Freire-Lista DM, Fort R, Varas-Muriel MJ. Thermal stress-induced microcracking in building granite. Eng Geol. 2016;206:83–93. https://doi.org/10.1016/j.enggeo.2016.03.005.

Gao B, Li Y, Pang Z, Huang T, Kong Y, Li B, Zhang F. Geochemical mechanisms of water/CO_2-rock interactions in EGS and its impacts on reservoir properties: a review. Geothermics. 2024;118:102923. https://doi.org/10.1016/j.geothermics.2024.102923.

Gautam PK, Verma AK, Jha MK, Sharma P, Singh TN. Effect of high temperature on physical and mechanical properties of Jalore granite. J Appl Geophys. 2018;159:460–74. https://doi.org/10.1016/j.jappgeo.2018.07.018.

Guo P, Bu M, Zhang P, Wang J, Luan Z, He M. Mechanical properties and crack propagation behavior of granite after high temperature treatment based on a thermo-mechanical grain-based model. Rock Mech Rock Eng. 2023;56:6411–35. https://doi.org/10.1007/s00603-023-03408-x.

Isaka BLA, Ranjith PG, Rathnaweera TD, Perera MSA, Kumari WGP. Influence of long-term operation of supercritical carbon dioxide based enhanced geothermal system on mineralogical and microstructurally-induced mechanical alteration of surrounding rock mass. Renew Energy. 2019;136:428–41. https://doi.org/10.1016/j.renene.2018.12.104.

Jiang C, Wang X, Zhang F, Deng K, Lei Q. Fracture activation and induced seismicity during long-term heat production in fractured geothermal reservoirs. Rock Mech Rock Eng. 2022;55:5235–58. https://doi.org/10.1007/s00603-022-02882-z.

Kao CS, Carvalho FCS, Labuz JF. Micromechanisms of fracture from acoustic emission. Int J Rock Mech Min. 2011;48:666–73. https://doi.org/10.1016/j.ijrmms.2011.04.001.

Kim K, Makhnenko RY. Short- and long-term responses of reservoir rock induced by CO_2 injection. Rock Mech Rock Eng. 2022;55:6605–25. https://doi.org/10.1007/s00603-022-03032-1.

Li H, Zhou L, Lu Y, Yan F, Zhou J, Tang J. Influence of supercritical CO_2 saturation on the failure process of hot dry rock with acoustic emission monitoring. Powder Technol. 2020;374:241–9. https://doi.org/10.1016/j.powtec.2020.07.006.

Li J, Guo Z, Ai D, Yang J, Wei Z. Nonlinear characteristics of granite after high-temperature treatment captured by digital image correlation and acoustic emission technology. Nat Resour Res. 2022;31:1307–27. https://doi.org/10.1007/s11053-022-10048-5.

Li P, Hao Y, Wu Y, Wanniarachchi A, Zhang H, Cui Z. Experimental study on the effect of CO_2 storage on the reservoir permeability in a CO_2-based enhanced geothermal system. Geotherm Energy. 2023a;11:24. https://doi.org/10.1186/s40517-023-00266-2.

Li W, Li Q, Qian Y, Ling F, Liu R. Structural properties and failure characteristics of granite after thermal treatment and water cooling. Geomech Geophys Geo-Energy Geo-Resour. 2023b;9:171. https://doi.org/10.1007/s40948-023-00716-y.

Liu S, Xu J. An experimental study on the physico-mechanical properties of two post-high-temperature rocks. Eng Geol. 2015;185:63–70. https://doi.org/10.1016/j.enggeo.2014.11.013.

Liu Z, Wang C, Zhang M, Shao JF. Cracking property and brittleness evaluation of granite under high-temperature true triaxial compression in geothermal systems. Geomech Geophys Geo. 2023;9:99. https://doi.org/10.1007/s40948-023-00631-2.
Miao S, Pan PZ, Zhao X, Shao C, Yu P. Experimental study on damage and fracture characteristics of Beishan granite subjected to high-temperature treatment with DIC and AE techniques. Rock Mech Rock Eng. 2021;54:721–43. https://doi.org/10.1007/s00603-020-02271-4.
Ré CL, Kaszuba JP, Moore JN, McPherson BJ. Fluid-rock interactions in CO_2-saturated, granite-hosted geothermal systems: implications for natural and engineered systems from geochemical experiments and models. Geochim Cosmochim Ac. 2014;141:160–78. https://doi.org/10.1016/j.gca.2014.06.015.
Rong G, Peng J, Cai M, Yao M, Zhou C, Sha S. Experimental investigation of thermal cycling effect on physical and mechanical properties of bedrocks in geothermal fields. Appl Therm Eng. 2018;141:174–85. https://doi.org/10.1016/j.applthermaleng.2018.05.126.
Shao S, Wasantha PLP, Ranjith PG, Chen BK. Effect of cooling rate on the mechanical behavior of heated Strathbogie granite with different grain sizes. Int J Rock Mech Min. 2014;70:381–7. https://doi.org/10.1016/j.ijrmms.2014.04.003.
Sun Q, Zhang W, Xue L, Zhang Z, Su T. Thermal damage pattern and thresholds of granite. Environ Earth Sci. 2015;74:2341–9. https://doi.org/10.1007/s12665-015-4234-9.
Tang C, Yao Q, Li Z, Zhang Y, Ju M. Experimental study of shear failure and crack propagation in water-bearing coal samples. Energy Sci Eng. 2019;7:2193–204. https://doi.org/10.1002/ese3.424.
Truche L, Bazarkina EF, Berger G, Caumon MC, Bessaque G, Dubessy J. Direct measurement of CO_2 solubility and pH in NaCl hydrothermal solutions by combining in-situ potentiometry and Raman spectroscopy up to 280 ℃ and 150bar. Geochim Cosmochim Ac. 2016;177:238–53. https://doi.org/10.1016/j.gca.2015.12.033.
Ueda A, Kato K, Ohsumi T, Yajima T, Ito H, Kaieda H, Metcalfe R, Takase H. Experimental studies of CO_2-rock interaction at elevated temperatures under hydrothermal conditions. Geochem J. 2005;39:417–25. https://doi.org/10.2343/geochemj.39.417.
Vázquez P, Shushakova V, Gómez-Heras M. Influence of mineralogy on granite decay induced by temperature increase: experimental observations and stress simulation. Eng Geol. 2015;189:58–67. https://doi.org/10.1016/j.enggeo.2015.01.026.
Wang F, Frühwirt T, Konietzky H. Influence of repeated heating on physical-mechanical properties and damage evolution of granite. Int J Rock Mech Min. 2020;136:104514. https://doi.org/10.1016/j.ijrmms.2020.104514.
Wang J, Zhang P, Bu M, Luan Z, Wang S. Mechanical behavior of granite subjected to thermal treatment: insight from experiment and numerical simulation. B Eng Geol Environ. 2023;82:400. https://doi.org/10.1007/s10064-023-03431-w.
Wu Y, Li P. The potential of coupled carbon storage and geothermal extraction in a CO_2-enhanced geothermal system: a review. Geotherm Energy. 2020;8:19. https://doi.org/10.1186/s40517-020-00173-w.
Wu Y, Li P, Hao Y, Wanniarachchi A, Zhang Y, Peng S. Experimental research on carbon storage in a CO_2-Based enhanced geothermal system. Renew Energy. 2021;175:68–79. https://doi.org/10.1016/j.renene.2021.04.139.
Wu Z, Li M, Xie H, Lu J, Chen C. Investigation on physico-mechanical properties and microstructural evolution patterns of heated granite after liquid nitrogen cooling. Geomech Geophys Geo. 2023;9:172. https://doi.org/10.1007/s40948-023-00720-2.
Xie H, Gao F, Ju Y. Research and development of rock mechanics in deep ground engineering. Chin J Rock Mech Eng. 2015;34:2161–78.
Xu X, Gao F, Zhang Z. Influence of high temperature on strength and deformation of granite. J Guangxi Univ. 2013;38:912–7.
Xu TF, Feng GH, Shi Y. On fluid-rock chemical interaction in CO_2-based geothermal systems. J Geochem Explor. 2014a;144:179–93. https://doi.org/10.1016/j.gexplo.2014.02.002.
Xu X, Gao F, Zhang Z. Temperature of brittle-ductile transition of granite under high temperature. Adv Sci Technol Water Resour. 2014b;34:43–8.
Yarushina VM, Bercovici D. Mineral carbon sequestration and induced seismicity. Geophys Res Lett. 2013;40:814–8. https://doi.org/10.1002/grl.50196.
Yin W, Feng Z, Zhao Y. Effect of grain size on the mechanical behaviour of granite under high temperature and triaxial stresses. Rock Mech Rock Eng. 2021;54:745–58. https://doi.org/10.1007/s00603-020-02303-z.
Yin W, Zhao Y, Feng Z. Effect of hydrothermal fluid backfill on the mechanical behavior of deep granite under high-temperature and high-pressure conditions. Rock Mech Rock Eng. 2023;56:4923–37. https://doi.org/10.1007/s00603-023-03310-6.
Zhang W, Sun Q, Hao S, Geng J, Lv C. Experimental study on the variation of physical and mechanical properties of rock after high temperature treatment. Appl Therm Eng. 2016;98:1297–304. https://doi.org/10.1016/j.applthermaleng.2016.01.010.
Zhao Y, Feng Z, Zhao Y, Wan Z. Experimental investigation on thermal cracking, permeability under HTHP and application for geothermal mining of HDR. Energy. 2017;132:305–14. https://doi.org/10.1016/j.energy.2017.05.093.
Zheng H, Feng X-T, Chen Z, Hudson JA, Wang Y. ISRM suggested method for reporting rock laboratory test data in electronic format. In: Ulusay R, editor. The ISRM suggested methods for rock characterization, testing and monitoring: 2007–2014. Cham: Springer International Publishing; 2015. p. 57–94.
Zhuang Q. Exploration, exploitation and utilization potential and countermeasures of dry hot rock geothermal resources in Fujian Province. Energy Environ. 2016;2:2–4.

Publisher's Note